IOP PUBLISHING PHYSICS IN MEDICINE AND BIOLOGY

Phys. Med. Biol. **53** (2008) 6979–6989 doi:10.1088/0031-9155/53/23/021

In vivo ^{19}F MRI and ^{19}F MRS of ^{19}F-labelled boronophenylalanine–fructose complex on a C6 rat glioma model to optimize boron neutron capture therapy (BNCT)

Paola Porcari[1,2], Silvia Capuani[1,2], Emanuela D'Amore[3], Mario Lecce[4], Angela La Bella[5], Fabrizio Fasano[6], Renzo Campanella[7], Luisa Maria Migneco[5], Francesco Saverio Pastore[4] and Bruno Maraviglia[2,8]

[1] CNR-INFM SOFT, Physics Department, University of Rome "Sapienza", Rome, Italy
[2] Enrico Fermi Center, Rome, Italy
[3] Service for Biotechnology and Animal Welfare, Istituto Superiore di Sanità, Rome, Italy
[4] Neuroscience Department, Institute of Neurosurgery, University of Rome "Tor Vergata", Rome, Italy
[5] Chemistry Department, University of Rome "Sapienza", Rome, Italy
[6] Neuroimaging Laboratory, Santa Lucia Foundation, IRCCS, Rome, Italy
[7] Physics Department, University of Perugia, Italy
[8] Physics Department, University of Rome "Sapienza", Rome, Italy

E-mail: paola.porcari@roma1.infn.it

Received 15 July 2008, in final form 13 October 2008
Published 12 November 2008
Online at stacks.iop.org/PMB/53/6979

Abstract

Boron neutron capture therapy (BNCT) is a promising binary modality used to treat malignant brain gliomas. To optimize BNCT effectiveness a non-invasive method is needed to monitor the spatial distribution of BNCT carriers in order to estimate the optimal timing for neutron irradiation. In this study, *in vivo* spatial distribution mapping and pharmacokinetics evaluation of the ^{19}F-labelled boronophenylalanine (BPA) were performed using ^{19}F magnetic resonance imaging (^{19}F MRI) and ^{19}F magnetic resonance spectroscopy (^{19}F MRS). Characteristic uptake of ^{19}F–BPA in C6 glioma showed a maximum at 2.5 h after compound infusion as confirmed by both ^{19}F images and ^{19}F spectra acquired on blood samples collected at different times after infusion. This study shows the ability of ^{19}F MRI to selectively map the bio-distribution of ^{19}F–BPA in a C6 rat glioma model, as well as providing a useful method to perform pharmacokinetics of BNCT carriers.

1. Introduction

Boron neutron capture therapy (BNCT) (Sauerwein 1993, Sweet 1997, Coderre and Morris 1999, Coderre *et al* 2003, Barth *et al* 2005, Pisarev *et al* 2007) is a binary radio-therapeutic modality mainly used for the treatment of malignant gliomas (anaplastic astrocytomas (AA) and glioblastoma multiforme (GBM)) (Soloway *et al* 1967, Hatanaka and Nakagawa 1994, Nakagawa and Hatanaka 1997, Van Rij *et al* 2005, Yamamoto *et al* 2008). These high-grade tumours are indeed among the most aggressive human brain cancers and are extremely resistant to all current forms of therapy (debulking surgery, conventional radiotherapy and chemotherapy). Their rapid growth and infiltrating nature leads shortly to tumour recurrence (80–90% of GBM recur locally) (Yamamoto *et al* 2008). As a consequence, malignant gliomas have a very poor prognosis with a median survival time (MST) ranging from 6 to 12 months.

Among the therapeutic strategies for the treatment of these primary brain tumours, BNCT holds a potential curative promise: it requires the *selective* accumulation of ^{10}B-labelled compounds in the tumour followed by the irradiation with low-energy ($E \leqslant 0.4$ eV) thermal (n_{th}) or epithermal (0.4 eV $< E <$ 10 keV) neutron beams. Specifically, BNCT is based on the nuclear reaction $^{10}\mathrm{B}(n, \alpha)^{7}\mathrm{Li}$ ($^{10}\mathrm{B} + n_{\mathrm{th}} \rightarrow [^{11}\mathrm{B}^{*}] \rightarrow \alpha + {}^{7}\mathrm{Li} + 2.79$ MeV) (Sauerwein 1993) that occurs when ^{10}B, a stable isotope (characterized by a large thermal neutron capture cross-section) captures a thermal neutron to yield ^{11}B in an unstable form, which immediately disintegrates into energetic α particles and recoiling ^{7}Li ions. Due to their high linear energy transfer (LET), these heavy charged particles release along their combined path lengths (<14 μm) (IAEA 2001) (comparable with mammalian cell dimensions) most of the ionizing energy, limiting therefore the radiation damage to cells containing ^{10}B. For effective BNCT a large amount of ^{10}B atoms (approximately 10^{9} atoms of ^{10}B per cell or 20–35 μg ^{10}B g^{-1}) (Barth and Soloway 1997) must be selectively accumulated within tumour cells while at the same time a high tumour-to-brain (T:Br) ^{10}B concentration ratio of at least 3:1 must be achieved to ensure a therapeutic dose to the tumour with a minimal background radiation dose.

BNCT therapy has been optimized and evaluated for safety and efficacy in several centres around the world (Coderre *et al* 1998, Chanana *et al* 1999, Capala *et al* 2003, Joensuu *et al* 2003, Miyatake *et al* 2007). Nevertheless the results of phase I (toxicity) (Chanana *et al* 1999, Palmer *et al* 2002, Busse *et al* 2003, Diaz 2003, Burian *et al* 2004) and phase II (efficacy) (Busse *et al* 2003, Diaz 2003, Enriksson *et al* 2008) clinical trials have not yet shown advantages to justify a randomized phase III study on BNCT. These unexciting results were mainly due to both the insufficient uptake of ^{10}B-labelled compound within tumour cells and to the lack of an effective imaging method to monitor the bio-distribution of ^{10}B-carriers in order to estimate the optimal timing of neutron irradiation (Kageji *et al* 2001). Moreover, due to the peculiarity of BNCT which is a biologically rather than geometrically targeted modality, the possible subclinical lesions, which cannot be imaged by definition, could be reached by the ^{10}B-labelled compound and underwent the desirable therapeutic effect. The ideal time for neutron irradiation is when the tumour-to-brain (T:Br) ^{10}B concentration ratio is at its maximum value.

Currently, the boron carrier most widely used in BNCT clinical trials is the boronated derivative of the essential amino acid phenylalanine, *p*-boronophenylalanine (BPA). Due to its low solubility at physiological pH, it is administrated as a complex with fructose (BPA–fr complex) (Yoshino *et al* 1989). It is widely accepted that BPA is actively transported across the blood–brain barrier into the normal glia while its uptake in the tumour is due to an elevated rate of amino acid transport across the tumour cell membrane (Wittig *et al* 2000). Moreover, BPA accumulation within tumour cells increases during the cell cycle (S phase) (Nichols *et al* 2002) so that its use for the treatment of brain gliomas might be an advantage.

Pharmacokinetics studies of ^{18}F-labelled BPA performed by positron emission tomography (PET) measurements, demonstrated a great rate of BPA intake in the tumour rather than in adjacent normal tissues as reported by Imahori *et al* (1998) and Kabalka *et al* (1997).

For BNCT effectiveness it is of critical importance to investigate the pharmacokinetic behaviour of ^{10}B carriers and to obtain their boron spatial bio-distribution in order to evaluate the efficiency of the carrier and the optimal irradiation time.

So far several techniques (Wittig *et al* 2008) have been used to determine the spatial distribution and pharmacokinetics of ^{10}B agents (Coderre *et al* 1998, Elowitz *et al* 1998, Imahori *et al* 1998, Ryynanen *et al* 2000, 2002, Laakso *et al* 2001, Kabalka *et al* 2003, Wang *et al* 2004). Among these, magnetic resonance imaging (MRI) and spectroscopy (MRS) are powerful and useful methodologies for *in vivo* non-invasive and non-destructive real-time monitoring of ^{10}B compounds during BNCT treatment. Nevertheless, due to the low sensitivity of the ^{10}B NMR method (Bendel *et al* 2001a, 2001b, Bendel 2005) and to the intense proton background signal that makes ^{1}H MRS (Zuo *et al* 1999) and magnetic resonance spectroscopy imaging (MRSI) (Bendel *et al* 2005) techniques problematic *in vivo*, new strategies to detect BPA by NMR are in progress. In a previous paper (Porcari *et al* 2006), we proposed a novel approach to detect BPA. The strategy used was to map ^{19}F-labelled BPA-fr complex (^{19}F–BPA–fr complex) using ^{19}F NMR in the similar way of PET studies (Imahori *et al* 1998, Kabalka *et al* 2003, Wang *et al* 2004). The feasibility of the method has been demonstrated *in vitro* (Porcari *et al* 2006). Nowadays, ^{19}F MRI probes (Bulte 2005, Higuchi *et al* 2005, Mizukami *et al* 2008) are very attractive for *in vivo* molecular imaging because of ^{19}F nuclide properties. Indeed, ^{19}F has natural isotopic abundance of 100%, high gyromagnetic ratio ($\gamma_F = 40.05$ MHz/T) and elevated NMR sensitivity (0.83 relative to ^{1}H). Moreover, due to ^{19}F and ^{1}H close γ values ($\gamma_F = 40.05$ MHz T^{-1}, $\gamma_H = 42.58$ MHz T^{-1}), ^{19}F NMR can be performed generally using ^{1}H NMR instruments by suitably tuning RF coils. This might be a very useful advantage for future clinical applications. Additionally ^{19}F-containing compounds, as ^{19}F–BPA–fr complex, having the capability of accumulating in specific sites, are administrated exogenously to the organism. Hence, they can be monitored *in vivo* without background magnetic resonance signal. Indeed, only few ^{19}F atoms are concentrated within living animals (mostly in the bones and teeth) so that the intrinsic ^{19}F MRI signal is hardly detectable. Recently, novel compounds containing both ^{19}F (also as trifluoromethyl group (Hattory *et al* 2007)) and ^{10}B atoms in a single molecule are designed and synthesized (Hattory *et al* 2006) for developing practical tools for both BNCT and MRI.

Aims of this study were: (1) to assess, using ^{19}F MRI, the selective bio-distribution of ^{19}F–BPA–fr complex in C6 tumour-bearing rats as compared with normal brain; (2) to evaluate, using ^{19}F MRI and MRS, the pharmacokinetics of ^{19}F-labelled BPA to estimate the optimal timing of neutron irradiation. The C6 rat glioma model was employed because it is well characterized and frequently used in similar studies even though there are substantial differences with human glioblastoma. In this paper, we report the first *in vivo* results obtained using ^{19}F–BPA–fr complex on C6 tumour-bearing rats. Specifically ^{19}F MRI images of rat brain, acquired after ^{19}F–BPA–fr complex administration to assess the spatial distribution mapping of the compound, and ^{19}F high-resolution NMR spectra of blood samples (collected from the femoral vein at different times after infusion), are reported.

2. Materials and methods

2.1. Chemicals

Racemic ^{10}B-enriched ^{19}F–BPA was purchased from Katchem Ltd (Prague, Czech Republic). Because of the ^{19}F–BPA poor water solubility, physiological solutions (pH = 7.4) for

administration to animals were prepared by complexing it with fructose (^{19}F–BPA–fr complex). The procedure of complexation with fructose has been described in detail elsewhere (Porcari *et al* 2006).

2.2. Animal model

2.2.1. Cell line. C6 cells (Istituto Zooprofilattico Sperimentale "B. Ubertini", Brescia, Italy) were cultured in Ham's F10 medium supplemented with 15% horse serum, 2.5% fetal calf serum and antibiotics (penicillin/streptomycin) in a humidified 5% CO_2/95% air at 37°C. All the materials for the culture medium were supplied by the Service for Biotechnology and Animal Welfare, Istituto Superiore di Sanità (Rome, Italy).

2.2.2. Tumour implantation. Brain gliomas were successfully induced in 8 week old male Wistar rats weighing 300–350 g (Service for Biotechnology and Animal Welfare, Istituto Superiore di Sanità, Rome, Italy). All procedures related to the animal care were performed in accordance with the Legislative Decree 116/92, which represents the Italian enforcement of the European Directive 86/609/EEC.

Before surgery, each rat was anaesthetized intraperitoneally with a mixture of ketamine (90 mg kg^{-1} b.w.; Ketavet 100, Intervet) combined with medetomidine hydrochloride (0.4 mg kg^{-1} b.w.; Domitor, Pfizer), and then placed into the stereotaxic frame (Stoelting Co., Wood Dale, IL, USA). A middle scalp incision was made and a small hole was drilled into the right hemisphere (2 mm anterior to the right coronal suture, 3 mm lateral to the sagittal suture). Special care was taken to keep the dura intact in order to prevent bleeding and cerebrospinal fluid leakage. Subsequently a C6 cell suspension (10^6 cells in 10 μl) was slowly injected (10 min), through the small drilled hole, at 4 mm depth from the dural layer using a Hamilton syringe (26-gauge needle). Two minutes after the end of injection the syringe was slowly removed. Then the burr hole was covered with candle wax, the operative field washed with saline solution and the scalp sutured. No complications occurred during the surgical procedure.

2.3. Magnetic resonance measurements

2.3.1. ^{19}F–BPA–fr complex infusion and MR imaging. *In vivo* proton and fluorine *imaging* was performed using a 7T horizontal bore MR-scanner (Bruker Biospec 70/15) equipped with a double-tuned ^{1}H–^{19}F surface coil (40 mm diameter, 50 mT m^{-1} maximum gradient strength, 800 ms rise time) suitable for small animals. Before imaging, each rat was anaesthetized (as above) and placed in supine position on the home-made rat bed. The surface coil was placed directly under the rat skull and centred over the bregma. The rat was then inserted into the magnet with the head positioned at the magnet isocenter. During MRI examination, the body temperature was maintained at 36–37 °C by a heating blanket.

Tumour implantation and progressive growth were monitored by ^{1}H MRI. Five days after C6 glioma cell implantation, rats were scanned for the first time and subsequently every 4 days. T2-weighted (T2-w) spin echo (SE) axial ^{1}H images of rat brain were performed with the following parameters: echo time (TE) = 40 ms, repetition time (TR) = 2500 ms, field of view (FOV) = 40 × 40 mm^2, matrix dimensions (MTX) = 128 × 128 (in plane resolution = 312 μm × 312 μm), number of average (NA) = 2 (total imaging time = 10 min), number of slices (NS) = 4, slice thickness (ST) = 1.5 mm. When the tumour size reached a minimum diameter of about 2 mm, rats were assigned to ^{19}F–BPA–fr complex administration. Before infusion, each rat was anaesthetized again (as described above) and surgically prepared by

neurosurgeons. The right internal carotid artery was cannulated (25-gauge Teflon catheter; Ethicon) and a ^{19}F–BPA–fr complex (300 mg kg^{-1} b.w.) solution was administered using an infusion pump (Harvard Apparatus Co., Cambridge, MA) at a constant low flow rate (100 μl min^{-1}). The catheter was then removed, the internal carotid artery ligated and the incision site sutured. During surgery and infusion two rats died for respiratory complications. *In vivo* ^{19}F–BPA spatial distribution mapping was performed using ^{19}F MRI. After the end of ^{19}F–BPA–fr complex infusion each rat underwent imaging using the same acquisition protocol. First, ^{1}H T2-w axial scans were collected for anatomical reference with the same acquisition parameters reported above. Then the coil was tuned to the ^{19}F frequency (282.35 MHz) and the corresponding ^{19}F MR brain axial images were obtained. Because of ^{19}F transverse relaxation time (T_2) of ^{19}F–BPA in blood was equal to 5.4 ms (Porcari *et al* 2006), SE sequence with 512 μs hermite 90° selective pulse and 200 μs hard 180° pulse was used to minimize TE. The acquisition parameters were as follows: TE = 4.3 ms, TR = 1800 ms, FOV = 120 × 120 mm^2, MTX = 64 × 64 (in plane resolution = 1.85 mm × 1.85 mm), NA = 40 (total imaging time = 77 min), NS = 1 and ST = 40 mm. ^{19}F MR acquisitions were started 2 h after the end of ^{19}F–BPA infusion and consecutive scans were collected over 4 h (specifically at 2.5, 4, and 5 h after infusion) in order to monitor the ^{19}F–BPA–fr complex bio-distribution. Afterwards T2-w ^{1}H axial scans were collected again (with the same acquisition parameter) to assess the rat position.

^{19}F–BPA–fr complex spatial distribution mapping was obtained by superimposing the ^{19}F MR image (in colour levels: low = blue, high = red) on the corresponding ^{1}H image (in grey levels). Both ^{1}H and ^{19}F images were processed using Matlab software (version 7.4, R 2007a). As the ^{19}F image was not slice selective, the ^{1}H image was obtained by overlapping the relevant proton slices. Conversely, ^{19}F image was re-sampled on the same ^{1}H image resolution (312 μm × 312 μm) using bicubic interpolation with threshold fixed to 70% of signal maximum value.

2.3.2. ^{19}F MR spectroscopy. To assess pharmacokinetic studies and to support the imaging data, blood samples were collected from the right femoral vein at different times (1, 2.5 and 4 h) after ^{19}F–BPA–fr-complex infusion. Each rat was surgically prepared and the right femoral vein was cannulated. Blood samples (each of 500 μl) were collected within heparin-coated cuvettes. In this case, one rat died during surgery because of haemorrhagic complications.

^{19}F NMR high-resolution spectra were collected on each blood sample using a 9.4 T vertical bore high-resolution spectrometer (Bruker Avance-400). All spectra were acquired with TR = 5 s, averaged with 4000 scans and processed with line broadening (LB) equal to 1 Hz exponential filter. Spectral quantification was achieved by peak integration. For each spectrum, the full-width at half-maximum value (FWHM) of all peaks were measured and the transverse relaxation time T_2^* (defined as FWHM = $1/(\pi\ T_2^*)$) was obtained.

3. Results and discussion

3.1. Imaging results

To assess *in vivo* boron distribution mapping of ^{19}F–BPA in the C6 animal model, the combination of ^{1}H and ^{19}F MRI was performed on ^{19}F–BPA infused rats. As shown by ^{1}H MRI monitoring, 14 days after C6 cells implantation each rat developed a brain tumour measuring about 2–3 mm in diameter. ^{1}H T2-w scans were collected for anatomical reference 2 h after ^{19}F–BPA infusion. In figure 1, three consecutive ^{1}H axial slices of rat brain covering tumour extension (arrowhead in figures 1(a)–(c)) are displayed. Immediately after ^{1}H MR acquisition, ^{19}F axial image of rat brain was obtained (figure 2). Due to the lack of ^{19}F

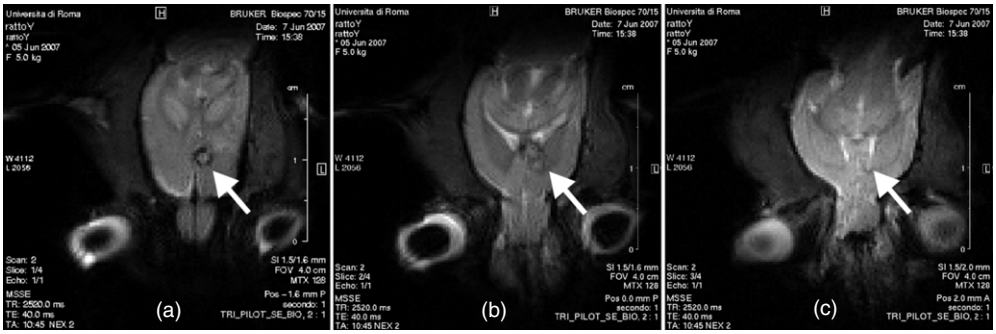

Figure 1. Axial ^{1}H MR images of rat brain acquired 2 h after the end of ^{19}F–BPA–fr complex infusion. Images (a)–(c) represent three consecutive slices positioned to cover the tumour extension. The tumour is indicated by white arrow in each image.

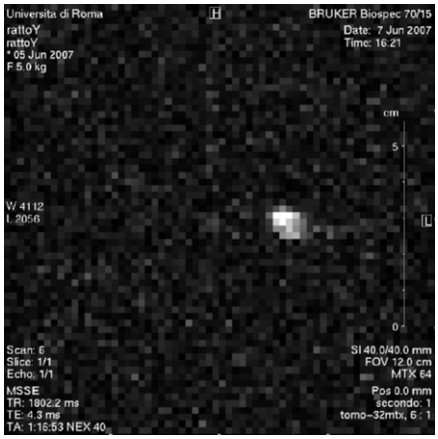

Figure 2. Axial ^{19}F MR image of rat brain acquired immediately after ^{1}H MR acquisition (as reported above).

background MR signal in brain tissue, the hyper-intense region in ^{19}F MR image (figure 2) derived only from the ^{19}F–BPA signal. In figure 3, selective spatial bio-distribution mapping of ^{19}F–BPA in C6 tumour-bearing rats is shown. ^{19}F image (in colour levels: low = blue, high = red) acquired 2.5 h after infusion (figure 2) was superimposed on the corresponding morphological ^{1}H reference (in grey levels). Indeed, the hyper-intense focus of ^{19}F–BPA uptake is coincident with the tumour site demonstrating a great specificity of ^{19}F–BPA carrier for C6 glioma cells. Furthermore a heterogeneous uptake of ^{19}F–BPA in both tumour and surrounding tissues was shown by ^{19}F colour map displayed in figure 3. Indeed, each colour represents (in the image processing) the percentage of ^{19}F magnetic resonance maximum signal above threshold (fixed at 70% as reported above).

To monitor the ^{19}F–BPA uptake in C6 glioma, consecutive ^{19}F MR axial scans were collected over 4 h on the same rat, respectively at 2.5 (figure 2(a)), 4 (figure 2(b)) and 5 h (figure 2(c)) after infusion. Signal-to-noise (S/N) ratio of each ^{19}F MR image was measured obtaining the following values: 5.1 (figure 4(a)), 3.7 (figure 4(b)) and 2.5 (figure 4(c)). These results demonstrate that ^{19}F–BPA in C6 tumour-bearing rat reaches the highest concentration at 2.5 h after infusion whilst after that time the concentration of the fluorinated compound decreases over time as shown in figures 4(b) and (c).

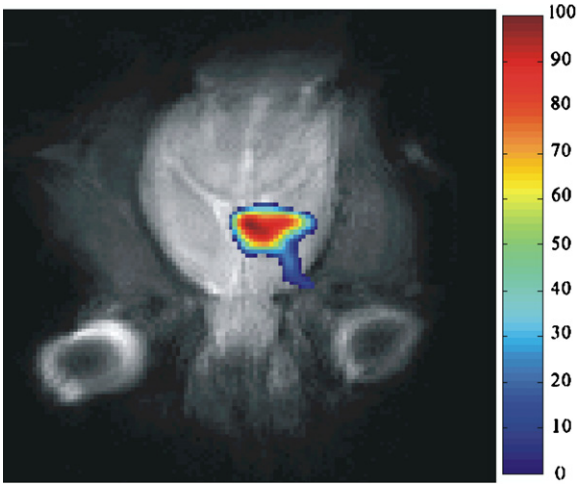

Figure 3. Superimposition of ^{19}F MR axial image of rat brain (in colour levels: low = blue, high = red) acquired 2.5 h after infusion on the corresponding morphological ^{1}H reference (in grey levels). The values reported close the colour look-up table represent the percentages of ^{19}F magnetic resonance maximum signal above threshold.

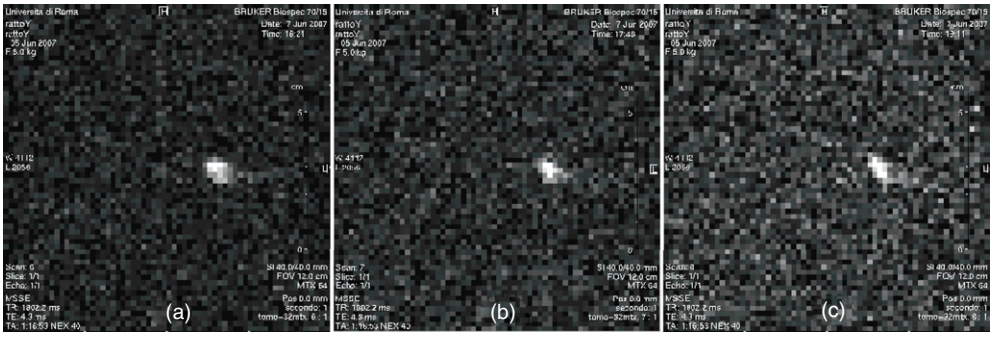

Figure 4. Progression of ^{19}F MR axial images of rat brain collected over 4 h on the same rat in order to monitor the ^{19}F–BPA–fr complex spatial distribution in C6 tumour-bearing rats. Images (a)–(c) represent three consecutive scans acquired 2.5, 4 and 5 h after infusion respectively.

Furthermore, no toxicity of ^{19}F–BPA–fr complex was assessed at the dosage infused. Indeed, all rats survived 2–3 weeks after infusion and died only for the tumour consequences.

3.2. Spectroscopic results

In figure 5, characteristic high-resolution ^{19}F NMR spectra of blood samples are reported. Spectra collected from the right femoral vein at 1, 2.5 and 4 h after the end of the ^{19}F–BPA–fr complex infusion are shown in figures 5(a)–(c), respectively. Since the ^{19}F–BPA–fr complex was in racemic form, the two major resonances in all spectra are reasonably due to the formation of two diastereomeric complexes.

All peaks displayed in figure 5 and belonging to the same spectrum showed roughly equal to FWHM. Specifically, the FWHM were equal to 61.04 Hz, 73.24 Hz and 24.41 Hz for peaks

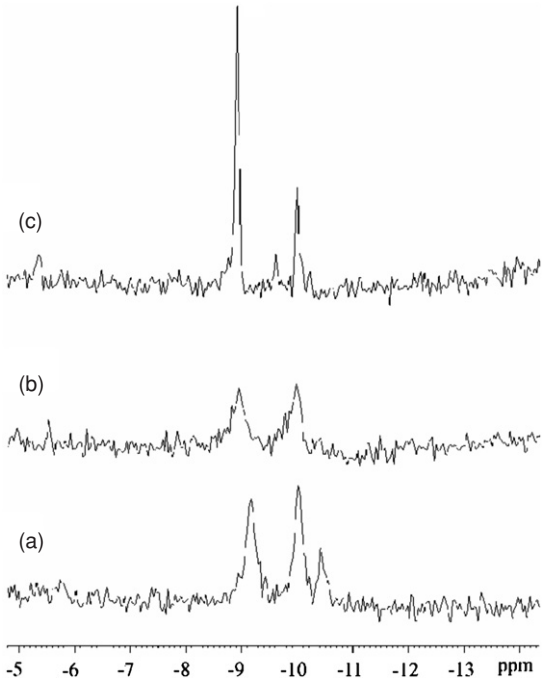

Figure 5. High-resolution ^{19}F NMR spectra of blood samples collected from the right femoral vein at 1 h (a), 2.5 h (b) and 4 h (c) after the ^{19}F–BPA–fr complex infusion.

displayed in figures 5(a)–(c) respectively. Besides the resultant T_2^* values were: 5.21 ms (figure 5(a)), 4.35 ms (figure 5(b)) and 13.04 ms (figure 5(b)).

It is interesting to compare these results. Indeed, T_2^* values of blood samples collected at 1 and 2.5 h after infusion are similar and both result slightly shorter than the transverse relaxation time T_2 (5.7 ms) obtained *in vitro* for ^{19}F–BPA–fr complex dissolved in blood solution (Porcari *et al* 2006).

Even if T_2^* is generally shorter than T_2, these findings suggest that 1 and 2.5 h after infusion the boron carrier in systemic circulation could be consistent with fluorinated BPA complexes. Conversely, T_2^* value of the blood sample collected 4 h after infusion (figure 5(c)) is considerably higher than those obtained on blood samples previously extracted (1 and 2.5 h after infusion). This observation could be consistent with a smaller molecule characterized by a faster molecular motion, which could be the result of ^{19}F–BPA–fr complex simplification due to the possible biological interactions and metabolic processes of the compound *in vivo*.

To evaluate the pharmacokinetics of ^{19}F–BPA–fr complex, spectral quantification was carried out either by peak integration or spectra difference. Quantification measurements showed that the total concentration of the fluorinated compound in the blood at 1 h after infusion (spectrum displayed in figure 5(a)) was approximately 22% higher than that observed in the blood at 2.5 and 4 h (figures 5(b) and (c) respectively) after the ^{19}F–BPA–fr complex infusion. Indeed the total concentration of fluorinated compound measured in the blood at 2.5 and 4 h after infusion was similar. These results show that the concentration of the fluorinated compound in systemic circulation decreases approximately of 22% from 1 to 2.5 h after infusion and then it remains constant until 4 h after infusion. It is interesting to compare

spectroscopic results on blood sample with imaging results on the rat brain. Specifically, the comparison between the spectrum displayed in figure 5(b) with the image shown in figure 4(a) demonstrates that 2.5 h after infusion the ^{19}F–BPA uptake is maximum in the tumour and minimum in systemic circulation. Conversely, the comparison between the spectrum displayed in figure 5(c) with the image shown in figure 4(b) shows that 4 h after infusion the concentration of the fluorinated compound in the tumour decreases whilst seems to be constant in the blood. This latter observation could be explained with the repetitive extractions of blood samples which contributes to the decrease of ^{19}F concentration in the blood. The combination of imaging and spectroscopic results demonstrates that the concentration of the fluorinated compound in the tumour increases until 2.5 h after the infusion and then decreases releasing the fluorine residues in the blood according to previous results (Hsieh *et al* 2005) obtained by means of PET measurements for ^{18}F-labelled BPA. These findings are very useful for BNCT clinical trials optimization.

4. Conclusion

In vivo experiments carried out in the present study demonstrate that ^{19}F MRI in combination with ^{1}H MRI can selectively map the bio-distribution of ^{19}F–BPA. Measurements were performed using the C6 rat glioma model because it was well characterized and commonly used in the literature to mimic the human glioblastoma. Furthermore, the results obtained by monitoring the ^{19}F BPA uptake in tumours using ^{19}F imaging strongly indicate ^{19}F MRI as a useful method to better understand and investigate the pharmacokinetics of fluorinated-containing drugs. Indeed, the correlation between the results obtained using ^{19}F MRI and ^{19}F MRS highlights an improved understanding of ^{19}F–BPA uptake in tumour and in systemic circulation showing, as a consequence, the optimal timing for neutron irradiation. These findings obtained on small rodents demonstrate that ^{19}F imaging and spectroscopy of ^{19}F–BPA are both feasible and practical methodologies with potential future applications for BNCT clinical trial. Moreover since ^{19}F NMR can be performed using a ^{1}H MR scanner by suitably tuning RF coils, future clinical applications would require only minor hardware and software MRI improvements to be carried out.

Acknowledgments

We gratefully acknowledge Professor Rinaldo Marini Bettolo (Chemistry Department, University of Rome “Sapienza”) for helpful discussion. We also thank Antonio Di Virgilio and Agostino Eusepi (Istituto Superiore di Sanità, Rome, Italy) for technical support.

References

Barth R F, Coderre J A, Vicente M G H and Blue T E 2005 Boron neutron capture therapy of cancer: current status and future prospects *Clin. Cancer Res.* **11** 3987–4002

Bendel P 2005 Biomedical application of ^{10}B and ^{11}B NMR *NMR Biomed.* **18** 74–82

Bendel P, Koudinova N and Salomon Y 2001a *In vivo* imaging of the neutron capture therapy agent BSH in mice using ^{10}B MRI *Magn. Reson. Med.* **46** 13–7

Bendel P, Margalit R and Salomon Y 2005 Optimized ^{1}H MRS and MRSI methods for the *in vivo* detection of boronophenylalnine *Magn. Reson. Med.* **53** 1166–71

Bendel P and Sauerwein W 2001b Optimal detection of the neutron capture therapy agent borocaptate sodium (BSH): a comparison between ^{1}H and ^{10}B NMR *Med. Phys.* **28** 178–83

Bulte J W 2005 Hot spot MRI emerges from the background *Nat. Biotechnol.* **23** 945–6

Burian J *et al* 2004 *Proc. of the 11th World Congress on Neutron Capture Therapy (Boston, USA 11–15 October 2004)* 27–32 Report on the first patient group of the phase I BNCT trial at the LVR-15 reactor

Busse P M *et al* 2003 A critical examination of the results from the Harvard-MIT NCT program phase I clinical trial of neutron capture therapy for intracranial disease *J. Neurooncol.* **62** 111–21

Capala J *et al* 2003 Boron neutron capture therapy (BNCT) for glioblastoma multiforme: clinical studies in Sweden *J. Neurooncol.* **62** 135–44

Chanana A D *et al* 1999 Boron neutron capture therapy for glioblastoma multiforme: interim results from the phaseI/II dose escalation studies *Neurosurgery* **44** 1182–93

Coderre J A and Morris G M 1999 The radiation biology of boron neutron capture therapy *Radiat. Res.* **151** 1–18

Coderre J A *et al* 1998 Biodistribution of boronophenylalanine in patients with glioblastoma multiforme: boron concentration correlates with tumor cellularity *Radiat. Res.* **149** 163–7

Coderre J A, Turcotte J C, Riley K J, Binns P J, Harling O K and Kiger W S 2003 Boron neutron capture therapy: cellular targeting of high linear energy transfer radiation *Tech. Cancer Res. Treat.* **2** 355–75

Diaz A Z 2003 Assessment of the results from the phase I/II boron neutron capture therapy trials at the Brookhaven National Laboratory from a clinician's point of view *J. Neurooncol.* **62** 101–9

Elowitz E H, Bergland R M, Coderre J A, Joel D D, Chandha M and Chanana A D 1998 Biodistribution of boronophenylalanine in patients with glioblastoma multiforme for use in boron neutron capture therapy *Neurosurgery* **42** 463–9

Enriksson R, Capala J, Michanek A, Lindahl S K, Salford L G, Franzen L, Blomquist E, Westlin J E, Bergenheim A T and Swedish Brain Tumour Study Group 2008 Boron neutron capture therapy (BNCT) for glioblastoma multiforme: a phase II study evaluating a prolonged high-dose of boronophenylalanine (BPA) *Radiother. Oncol.* **88** 183–91

Hatanaka H and Nakagawa Y 1994 Clinical results of long-surviving brain tumor patients who underwent boron neutron capture therapy *Int. J. Radiat. Oncol. Biol. Phys* **28** 1061–6

Hattory Y, Asano T, Niki Y, Kondoh H, Kirihata M, Yamaguchi Y and Wakamiya T 2006 Study on the compounds containing ^{19}F and ^{10}B atoms in a single molecule for the application to MRI and BNCT *Bioorg. Med. Chem.* **14** 3258–62

Hattory Y, Yamamoto H, Ando H, Kondoh H, Asano T, Kirihata M, Yamaguchi Y and Wakamiya T 2007 Synthesis and evaluation as MRI probe of the trifluoromethylated *p*-boronophenylalanine and its alcohol derivative *Bioorg. Med. Chem.* **15** 2198–205

Higuchi M, Iwata N, Matsuba Y, Sato K, Sasamoto K and Saido T C 2005 ^{19}F and ^{1}H MRI detection of amyloid beta plaques *in vivo Natl Neurosci.* **8** 527–33

Hsieh C H, Chen Y F, Chen F D, Hwang J J, Chen J C, Liu R S, Kai J J, Chang C W and Wang H E 2005 Evaluation of pharmacokinetics of 4-borono-2–^{18}F-fluoro-L-phenylalanine for boron neutron capture therapy in a glioma-bearing rat model with hyperosmolar blood-brain barrier disruption *J. Nucl. Med.* **46** 1858–65

Imahori Y, Ueda S, Ohmori Y, Kusuki T, Ono K, Fujii R and Ido T 1998 Fluorine-18-labeled fluoroboronophenylalanine PET in patients with glioma *J. Nucl. Med.* **39** 325–33

International Atomic Energy Agency IAEA 2001 *Current status of neutron capture therapy* (Vienna: IAEA Press) IAEA-TECDOC-1223

Joensuu H *et al* 2003 neutron capture therapy of brain tumors: clinical trials at the Finnish facility using boronophenylalanine *J. Neurooncol.* **62** 123–34

Kabalka G W, Smith G T, Dyke G P, Reid W S, Longford C P, Roberts T G, Reddy N K, Bonocore E and Hubner K F 1997 Evaluation of fluorine-18-BPA-fructose for boron neutron capture treatment planning *J. Nucl. Med.* **38** 1762–7

Kabalka W G, Nichols T L, Smith G T, Miller L F, Khan M K and Busse P M 2003 The use of positron emission tomography to develop boron neutron capture therapy treatment plans for metastatic malignant melanoma *J. Neurooncol.* **62** 187–95

Kageji T, Nagahiro S, Kitamura K, Nakagawa Y, Hatanaka H, Haritz D, Grochulla F, Haselsberger K and Gabel D 2001 Optimal timing of neutron irradiation for boron neutron capture therapy after intravenous infusion of sodium borocaptate in patients with glioblastoma *Int. J. Radiat. Oncol. Biol. Phys* **51** 120–30

Laakso J, Kulvik M, Ruokonen I, Vahatalo J, Zilliacus R, Farkkila M and Kallio M 2001 Atomic emission method for total boron in blood during neutron capture therapy *Clin. Chem.* **47** 1796–803

Miyatake S, Tamura Y, Kawabata S, Iida K, Kuroiwa T and Ono K 2007 Boron neutron capture therapy for malignant tumors related to meningiomas *Neurosurgery* **61** 82–90

Mizukami S, Takikawa R, Sugihara F, Hori Y, Tochio H, Walchli M, Shirakawa M and Kikuchi K 2008 Paramagnetic relaxation-based ^{19}F MRI probe to detect protease activity *J. Am. Chem. Soc.* **130** 794–5

Nakagawa Y and Hatanaka H 1997 Boron neutron capture therapy. Clinical brain tumor studies *J. Neurooncol.* **33** 105–15

Nichols T L, Kabalka G W, Miller L F, Khan M K and Smith G T 2002 Improved treatment planning for boron neutron capture therapy for glioblastoma multiforme using fluorine-18 labeled boronophenylalanine and positron emission tomography *Med. Phys.* **29** 2351–8

Palmer M R, Goorley J T, Kiger W S, Busse P M, Riley J K, Harling O K and Zamenhof R G 2002 Treatment planning and dosimetry for the Harvard-MIT Phase I clinical trial of cranial neutron capture therapy *Int. J. Radiat. Oncol. Biol. Phys.* **53** 1361–79

Pisarev M A, Dagrosa M A and Juvenal G J 2007 Boron neutron capture therapy in cancer: past, present and future *Arq. Bras. Endocrinol. Metab.* **51** 852–6

Porcari P, Capuani S, Campanella R, La Bella A, Migneco L M and Maraviglia B 2006 Multi-nuclear MRS and ^{19}F MRI of ^{19}F-labelled and ^{10}B-enriched *p*-boronophenylalanine-fructose complex to optimize boron neutron capture therapy: phantom study at high magnetic field *Phys. Med. Biol.* **51** 3141–54

Ryynanen P, Kangasmaki A, Hiismaki P, Coderre J A, Diaz A Z, Kallio M, Laakso J, Kulvik M and Savolainen S 2002 Non linear models for the kinetics of ^{10}B in blood after BPA-fructose complex infusion *Phys. Med. Biol.* **47** 737–45

Ryynanen P, Kortesnieni M, Coderre J A, Diaz A Z, Hiismaki P and Savolainen S 2000 Models for estimation of the ^{10}B concentration after BPA-fructose complex infusion in patient during epithermal neutron irradiation in BNCT *Int. J. Radiat. Oncol. Biol. Phys.* **48** 1145–54

Sauerwein W 1993 Principles and history of neutron capture therapy *Strahlenther. Onkol.* **169** 1–6

Soloway A H, Hatanaka H and Davis M A 1967 Penetration of brain and brain tumor. VII. Tumor-binding sulfhydryl boron compounds *J. Med. Chem.* **10** 714–7

Sweet W H 1997 Early history of development of boron neutron capture therapy of tumors *J. Neurooncol.* **33** 19–26

Van Rij C M, Wilhelm A J, Sauerwein W A G and Van Loenen A C 2005 Boron neutron capture therapy for glioblastoma multiforme *Pharm. World Sci.* **27** 92–95

Wang H L, Liao A H, Deng W P, Chang P F, Chen J C, Chen F D, Liu R S, Lee J S and Hwang J J 2004 Evaluation of 4-Borono- 2- ^{18}F-Fluoro-L-Phenylalanine-Fructose as a probe for boron neutron capture therapy in a glioma-bearing rat model *J. Neurooncol.* **45** 302–8

Wittig A, Michel J, Moss R L, Stecher-Rasmussen F, Arlinghaus H F, Bendel P, Mauri P L, Altieri S, Hilger R, Salvadori P A, Menichetti L, Zamenhof R and Sauerwein WAG 2008 Boron analysis and boron imaging in biological materials for Boron Neutron Capture Therapy *Crit. Rev. Oncol. Hematol* **68** 66–90

Wittig A, Sauerwein W A and Coderre J A 2000 Mechanisms of transport of p-borono-phenylalanine through the cell membrane *in vitro Radiat. Res.* **153** 173–80

Yamamoto T, Nakai K and Matsumura A 2008 Boron neutron capture therapy for glioblastoma *Cancer Lett.* **262** 143–52

Yoshino K, Suzuki A, Mori Y, Kakiana H, Honda C, Mishima Y, Kobayashi T and Kanda K 1989 Improvement of solubility of *p*-boronophenylalanine by complex formation with monosaccharides *Strahlenther. Onkol.* **165** 127–9

Zuo C S, Prasad P V, Busse P, Tang L and Zamenhof R G 1999 Proton nuclear magnetic resonance measurement of *p*-boronophenylalnine (BPA): a therapeutic agent for boron neutron capture therapy *Med. Phys.* **26** 1230–6